Tissue-selective restriction of RNA editing of Ca$_V$1.3 by splicing factor SRSF9

Hua Huang[1,2,*], Katannya Kapeli[1], Wenhao Jin[1], Yuk Peng Wong[1,2],
Thiruma Valavan Arumugam[1], Joanne Huifen Koh[1], Sumitra Srimasorn[1],
Karthik Mallilankaraman[1], John Jia En Chua[1,2,3], Gene W. Yeo[1,4,5] and Tuck Wah Soong[1,2,*]

[1]Department of Physiology, Yong Loo Lin School of Medicine, National University of Singapore, Singapore 117597, Singapore, [2]Neurobiology/Ageing Programme, Life Sciences Institute, National University of Singapore, Singapore 117456, Singapore, [3]Institute of Molecular and Cell Biology, Agency for Science, Technology and Research (A*STAR), Singapore 138673, Singapore, [4]Department of Cellular and Molecular Medicine, Stem Cell Program and Institute for Genomic Medicine, University of California, San Diego, La Jolla, USA and [5]Molecular Engineering Laboratory, A*STAR, Singapore, Singapore

ABSTRACT

Adenosine DeAminases acting on RNA (ADAR) catalyzes adenosine-to-inosine (A-to-I) conversion within RNA duplex structures. While A-to-I editing is often dynamically regulated in a spatial-temporal manner, the mechanisms underlying its tissue-selective restriction remain elusive. We have previously reported that transcripts of voltage-gated calcium channel Ca$_V$1.3 are subject to brain-selective A-to-I RNA editing by ADAR2. Here, we show that editing of Ca$_V$1.3 mRNA is dependent on a 40 bp RNA duplex formed between exon 41 and an evolutionarily conserved editing site complementary sequence (ECS) located within the preceding intron. Heterologous expression of a mouse minigene that contained the ECS, intermediate intronic sequence and exon 41 with ADAR2 yielded robust editing. Interestingly, editing of Ca$_V$1.3 was potently inhibited by serine/arginine-rich splicing factor 9 (SRSF9). Mechanistically, the inhibitory effect of SRSF9 required direct RNA interaction. Selective down-regulation of SRSF9 in neurons provides a basis for the neuron-specific editing of Ca$_V$1.3 transcripts.

INTRODUCTION

The information content within a mammalian genome is amplified through post-transcriptional and post-translational modifications, resulting in RNA transcripts and proteins with diverse structures and functions that are essential for survival and adaptation. The most prevalent form of RNA editing in the mammalian system is mediated by *A*denosine *DeA*minases acting of *R*NA (ADAR) that converts adenosine to inosine (A-to-I). The mammalian ADAR family comprises of ADAR1 to 3. While ADAR1 and ADAR2 are catalytically active and show overlapping specificity, ADAR3 has no known targets.

ADAR proteins were initially described for their ability to unwind double-stranded RNA (dsRNA) (1,2). More recently, ADAR proteins are appreciated for affecting A-to-I editing to exert a myriad of effects ranging from the modulation of splice site selection (3,4), targeting of microRNAs (5–9) to the processing of long non-coding RNAs (10,11). Notably, as inosine is decoded as guanosine by the ribosomal translational complex, A-to-I editing in coding exons specifies a single nucleotide change that may alter the codon to encode a different amino acid, thereby producing a protein variant with altered functional property.

Physiologically, deletion of ADAR1 in mouse has been shown to lead to embryonic morbidity (12) while ADAR2 knockout mice die at P20 due to epilepsy (13). Although the lethal phenotype of $ADAR2^{-/-}$ could be rescued by transgenic expression of edited GluR-B$^{R/R}$ subunits, additional phenotypic changes in behavior, hearing, allergy and altered gene expression have been reported, arguing for the physiological importance of the other ADAR2-mediated editing events (14). In human, disruption of A-to-I RNA editing levels has been associated with diseases such as depression, amyotrophic lateral sclerosis and cancers (15).

We have previously reported that transcripts of voltage-gated Ca$_V$1.3 calcium channel were subjected to A-to-I RNA editing specifically within exon 41(16). RNA editing occurs at three closely spaced adenosines, yielding non-synonymous changes that alter amino acid sequences within

the critical C-terminal IQ-domain of the channel. We have also shown that RNA editing of $Ca_V1.3$ required ADAR2 and edited channels are inactivated with much slower kinetic, leading to higher firing frequency of action potentials in the neurons of the superchiasmatic nucleus (SCN) [16]. More recently, downregulation of editing in $Ca_V1.3$ transcripts was reported in the hippocampus of Alzheimer's disease patient, emphasizing its disease relevance [17].

Remarkably, A-to-I editing of $Ca_V1.3$ transcripts was found to be restricted to neuronal tissues [16] and such a phenomenon is puzzling given the ubiquitous expression of $Ca_V1.3$ channels and ADAR2. Partly, it could be explained by other mechanisms that exist to regulate ADAR2 activity. For instance, ADAR2 expression could be promoted by CREB1 activation [18]. Secondly, ADAR2 transcripts could be subjected to different post-transcriptional modifications, giving rise either to non-coding transcripts or less active variants of the enzyme [3,19–21]. On the protein level, peptidyl prolyl isomerase (Pin1) reportedly stimulates ADAR2 activity by ensuring nuclear localization and stability of ADAR2 while E3 ubiquitin ligase WWP2 downregulates ADAR2 by catalysing its ubiquitination [22].

However, regulation of either the expression level or activity of ADAR2 alone fails to explain the different editing efficiencies among ADAR2 substrates [13,23]. In fact, substantial editing of some ADAR2 substrates such as GluR-B Q/R and $5HT_{2C}$ receptor editing site D was observed even before ADAR2 expression was detectable during development [23]. Alternatively, it was recently reported that RNA binding factors such as ribosomal protein S14 (RPS14), serine/arginine-rich splicing factor 9 (SFRS9) and DEAH box polypeptide 15 (DHX15) could suppress ADAR2-mediated A-to-I editing in a substrate selective manner, although the detailed molecular mechanism have not been completely elucidated [24].

The current work seeks to understand the molecular mechanisms that restrict A-to-I RNA editing of the $Ca_V1.3$ transcript. Firstly, we showed that editing of $Ca_V1.3$ transcripts required a 40 bp duplex RNA structure that forms between exon 41 and the complementary ECS sequence within the preceding intron. Secondly, we demonstrated that co-expression of a mouse minigene spanning ECS, intermediate intronic sequence and exon 41 with ADAR2 permitted robust editing which was potently inhibited by SRSF9. Mechanistically, we elucidated that SRSF9 disrupted ADAR2 activity via direct RNA interaction. Notably, *Srsf9* transcript and SRSF9 protein levels were drastically downregulated in cultured neurons and in different brain tissues, thus correlating with neuron-specific editing of $Ca_V1.3$ transcripts. Moreover, editing of endogenous $Ca_V1.3$ was reduced upon overexpression of wildtype, but not RNA binding mutant, SRSF9 in primary neuronal culture via viral transduction. Accordingly, our experiments identified that splicing factor SRSF9 is a potent suppressor of ADAR2-mediated $Ca_V1.3$ RNA editing and provided strong evidence that a cell-type specific down-regulation of such a RNA editing suppressor could contribute toward an overall upregulation and a tissue-selective RNA editing of $Ca_V1.3$ RNA in neurons.

MATERIALS AND METHODS

Construction of minigenes for *in vitro* A-to-I editing assay

The minigene gIQECS was generated by ligating a SpeI-XhoI genomic DNA fragment digested from mouse bacterial artificial chromosome (Library Plates 481, ResGen, USA, CA) into the modified pRK5 vector digested by XbaI and SalI. The 4952 bp genomic DNA contains the putative ECS, intermediate sequence and exon 41. The modified PRK5 vector was generously provided by Dr Miyoko Higuchi from Max-Planck Institute for Medical Research, Germany. Subsequently, in the same vector the ECS sequence was deleted from by overlapping PCR to produce the gIQΔECS minigene and the short IQECS minigene that supports the expression of only the RNA duplex was constructed by PCR prior to cloning into the modified pRK5 vector. All restriction enzymes, DNA Polymerase I, Large (Klenow) Fragment and T4 DNA ligase were purchased from New England Biolabs, USA and used per manufacturer's instruction.

Cloning of ADAR2, RPS14, DHX15, SRSF9 and mutants

The pRK5-RED1 expression vector expressing FLAG-tagged rat ADAR2 was kindly provided by Dr. Miyoko Higuchi of the, Max Planck Institute of Biomedical Research, and it was subsequently recloned by into pIRES2-EGFP (Clontech, Mountain View, CA, USA) to allow for monitoring the expression efficiency. Human RPS14, DDX15 and SRSF9 were cloned by PCR using human brain cDNA (Clontech, Marathon- ready™ cDNA) as template with the following primer pairs, RPS14_F (GCTAGCATGGCACCTCGAAAGGGGAA) and RPS14_R (GGATCCCTACAGACGGCGACCACGGC), DHX15_F (GCTAGCATGCTTATCAGTGCTGGATT) and DHX15_R (GGATCCTCAGTACTGTGAATATTCCTT), SRSF9_F (GCTAGCATGTCGGGCTGGGCGGACGA) and SRSF9_R (GGATCCCTAGTAGGGCCTGAAAGGAGA) respectively. The deletion mutants of SRSF9 were generated by PCR while point mutants of SRSF9 were generated by circular mutagenesis with Pfu-Turbo DNA polymerase (Stratagene, La Jolla, CA). To facilitate co-immunoprecipitation, a hemagglutinin (HA) tag sequence TACCCATACGATGTTCCAGATTACGCT was inserted before the stop codon of RPS14, DHX15, SRSF9 and relevant variants by PCR.

Transfection of cell-lines

HEK293 cells (ATCC, USA) cultured in DMEM with 10% (v/v) FBS in 6-well plate were transfected by calcium phosphate method as reported previously [16]. 0.1 ug of respective minigene reporters including gIQECS, gIQΔECS or IQECS was co-transfected with 1 μg of ADAR2, 0.25 μg of TAG construct [25] and 2 μg of either empty pIRES2 DsRed-Express2 vectors or putative ADAR2 suppressors, amount otherwise indicated. SH-SY5Y cells (ATCC, USA), at 50% confluency in 6-well plate, were cotransfected with 1 μg of ADAR2 and 2 μg of either empty pIRES2 DsRed-Express2 vectors or putative ADAR2 suppressors, using

Lipofectamine 2000 (Invitrogen, Carlsbad, CA, USA) according to manufacturer's protocol.

RNA extraction and preparation of cDNA

Total RNA was isolated using the Trizol method (Invitrogen, Carlsbad, CA, USA). The RNA samples were treated with RNase-free DNase (Ambion, USA) before reverse transcription. For $Ca_V1.3$ minigene RNA, first strand cDNA was synthesized with Superscript III (Invitrogen, Carlsbad, CA) and reverse primers cis33 (GCGGTACCAATAAACAAGTTGGGCCATGG) specific to within SV40 polyadenylation signal in the modified pRK5 vector. For native human $Ca_V1.3$ RNA in SH-SY5Y cells and rodent $Ca_V1.3$ in native tissues or primary cell culture, reverse transcription was performed with oligo (dT)18 primers. Negative controls were performed without reverse transcriptase, together with all reverse transcription RT-PCR experiments, to exclude contamination by genomic DNA.

Transcript-scanning and quantification of editing

To assay for editing level of minigene transcripts gIQECS and gIQΔECS, PCR was performed with the primers pair, GP1 (GGTGGCGCTTCCTATCGTTA) and GP2 (AGGGGCAGTGGGCAGTATCTC) and the PCR amplicons were sequenced with GP3 (TGCCCCCAGCCAGAAGT). For IQECS, the primer pairs Mini_Fwd (TCTAGATCCTCTCAACTCTC) and Mini_Rev (GTCGACTCCGTTTCTTGAATTTC) were used and sequencing was performed with Mini_Fwd. To screen for editing level of native human $Ca_V1.3$ in SH-SY5Y cells, primer pairs Hum_Fwd (CTTTGGTTCGAACGGCTCTTA) and Hum_Rvs (TGTAGGGCAATTGTGGTGTTCT) were used and sequencing was performed with Hum_Fwd primer. To screen for editing level of native $Ca_V1.3$ in mouse cells and tissues, primer pairs Mouse_Fwd (GAACCTGGAGCAAGCTAATGAAG) and Mouse_Rvs (CTGTAGGGCAATCGTGGTGTT) were used. To screen for editing level of native $Ca_V1.3$ in rat cortical neurons cells, primer pairs Rat_Fwd (GCAACCTGGAGCAAGCTAATG) and Rat_Rvs (ATCGTGGTGTTCTTCGCAGG) were used.

PCR reactions were performed with GoTaq® Green Master Mix (Promega,. Madison, WI, USA) according to manufacturer's protocol. PCR products were separated in a 1.5% agarose gel, and isolated and purified using the QIAGEN gel extraction kit. The PCR products were sent for automated DNA sequencing (1st base, Singapore). Subsequently, DNA chromatograms were analyzed by Lasergene software (DNASTAR, Madison, WI, USA) Percent editing was calculated by dividing heights for adenosine peak over the total height of the overlapping adenosine and guanosine peaks.

Culturing of primary mouse, rat cortical neurons and mouse astrocytes

The protocol for generating cortical neurons has been described (26). Briefly, mouse cortical tissues were obtained from 16 day *C57BL/6NTac* fetuses and incubated for 15 min in a solution of 2 mg/ml trypsin in-Ca^{2+}/Mg^{2+}-free Hank's balanced salt solution (HBSS) buffered with 10 mmol/l HEPES (Invitrogen, Carlsbad, CA, USA). The cortical tissue was rinsed once in HBSS, followed by 5 min incubation in HBSS containing 1 mg/ml trypsin inhibitor (Sigma-Aldrich), and a final rinse in HBSS. Tissues were dissociated by trituration through the narrowed bore of a fire-polished Pasteur pipette. The neurons were cultured on polylysine-coated plastic culture dishes (Corning, Lowell, MA, USA) in solutions containing 2 ml of Eagle's minimum essential medium (Invitrogen) buffered with 10 mmol/l sodium bicarbonate and supplemented with 10% (v/v) with fetal bovine serum (Sigma-Aldrich), 2 mmol/l L-glutamine, 20 mmol/l KCl, 1 mmol/l pyruvate and 40 mmol/l glucose. The culture density was 80–120 cells/mm of culture surface. Cultures were maintained at 37°C in a 6% CO_2/94% room air, humidified incubator. All experiments were performed with neurons that had been in culture for 8–15 days.

Rat cortical neurons were obtained from dissection of P1 pups as previously described (27) using the Papain Dissociation System (Worthington Cat# LK003150). Briefly, the cortices were dissected and titrated 10 times in papain solution and incubated at 37°C for 40 min. The cell suspension was then centrifuged at 1000 rpm, 4°C for 10 min. After removing the supernatant, the pellet was suspended in STOP solution (DNase, papain inhibitor and Earle's Balanced Salt Solution, EBSS). The cells were then titrated and left at room temperature for 10 min. The mixture was layered on top of the 10/10 solution (Bovine Serum Albumin, BSA and trypsin inhibitor in EBSS) and then centrifuged at 1000 rpm, 4°C for 10 min. The cortical neuronal culture were plated in culture plate wells previously coated with poly-D-lysine (Sigma-Aldrich Cat#P6407), and maintained in Dulbecco's Modified Eagle's Medium/Nutrient Mixture F-12 Ham (Sigma-Aldrich Cat#D6421) supplemented with B-27 supplement (Thermofisher Scientific Cat#17504-044).

Primary astrocyte cell cultures were prepared from neonatal *C57BL6/NTac* mice. Neonatal mice were sacrificed by cervical dislocation within two days of birth, and the brains harvested. The meninges were removed and the remaining tissue was placed in HBSS and dissociated by passing through a 20-gauge needle several times. The collected cells were re-suspended in culture medium (MEM; 1% penicillin/streptomycin; 0.2 mM L-glutamine; 10% FBS) and plated in 75 cm² flask. The cells were incubated in a humidified incubator at 37°C and 5% CO_2. After 24 h, the non-adherent cells were removed and cells were incubated in culture medium for 10 days with a medium change every 3–4 days. After 10 days, microglial cells were removed and remaining cells were incubated in culture medium for 10 days without a medium change.

Construction of Lenti vector construct, viral particle production and infection

The coding sequences for HA-tagged SRSF9_WT and SRSF9_{FF-DD_5A} were introduced into LentiCRISPRv2 GFP (28) to replace the Cas9-P2A-EGFP sequence using the XbaI and BsrGI restriction enzymes, yielding Lenti-

SRSF9$_{WT}$ and Lenti- SRSF9$_{FF-DD\_5A}$ vectors, respectively. LentiCRISPRv2GFP was a gift from David Feldser (Addgene plasmid 82416). To generate the control Lenti-control vector, the XbaI and BsrGI digested vector was blunt-ended with Klenow fragment (NEB) and ligated. The three constructs Lenti-control, Lenti-SRSF9$_{WT}$ and Lenti-SRSF9$_{FF-DD\_5A}$ were cotransfected with the packaging plasmid pMDLg/pRRE (expressing HIV-1 gag/pol), pRSV-Rev and pMD2.G (encoding the vesicular stomatitis virus glycoprotein (VSV-G) into human embryonic kidney 293 cells using polyethylenimine (PEI). The pMDLg/pRRE, pRSV-Rev and pMD2.G plasmids were gifts from Didier Trono (Addgene plasmids 12251, 12253 and 12259).

Lentivirus-containing cell culture supernatant was harvested 30 h post-transfection and filtered through a 0.45 µm PES filter. Fifteen ml of diluted virus were subsequently concentrated by Amicon Untra-15 Centrifugal Filters (Merck Millipore Cat#UFC901024) and resuspended with 1.5 ml of neuronal culture medium. To infect rat cortical neurons, viruses were introduced to the cells at DIV3 and DIV5 in the presence of 2 µg/ml polybrene (Sigma-Aldrich Cat# H9268). The cells were harvested for experiments at DIV11.

Nuclear and cytoplasmic fractionation

Nuclear and cytoplasmic fractions were prepared with nuclear extraction kit (ab113474, Abcam) as per manufacturer's protocol.

Mouse tissue isolation

Various mouse tissues including mouse brain cortex, hippocampus, cerebellum, heart, lung, adrenal gland, kidney and testis were obtained from 3-month-old *C57BL/6* mice by dissection, and tissues were subsequently snap-frozen in liquid nitrogen.

RT-PCR analysis of *Srsf9* mRNA

Srsf9 expression were detected with the primers Srsf9_Fwd (TGCGCGAGAAGGACCTCG) and Srsf9_Rvs (AGGAGAGAAGTAGTGTGGCGA).

Western blot detection of ADAR2, SRSF9 and Lamin B1 in native tissues

Approximately 50–100 mg of various mouse tissues including brain cortex, heart, lung, adrenal gland, kidney and testis were homogenized and lysed in 1 ml RIPA lysis buffer by a Dounce homogenizer (50 strokes) at 4 ˚C. RIPA buffer consists of 150 mM sodium chloride, 0.1% Trion X-100, 0.5% sodium deoxycholate, 0.1% SDS and 50 mM Tris, pH 8.0 supplemented with Mini, EDTA-free Protease Inhibitor Cocktail (Roche). The lysates were further rotated at 4 ˚C for 2 h prior to sonication with VCX ultrasonic processors (Sonic & Materials, USA) at 50% amplitude for 3 × 10 s pulses. The lysate were centrifuged at 12 000 g for 20 min, and the supernatant was harvested and 120 to 240 µg of protein were loaded for SDS-PAGE. Anti-ADAR2 (Abcam, ab64830), SRSF9 (MBL, RN081PW) and LAMIN B1 (Abcam, ab16048) antibodies were used in the dilution of 1:1000.

Pull-down of SRSF9 and relevant variants with SBP-tagged ADAR2

The streptavidin binding peptide (SBP)-tag (MDEKTTGW RGGHVVEGLAGELEQLRARLEHHPQGQREP) (29) was genetically engineered to fuse to the C-terminal of ADAR2 by PCR to generate the ADAR2-SBP clone. 1 µg of ADAR2-SBP and 2 µg of SRSF9 and relevant variants were transfected into HEK 293 cells cultured on six-well plates. About 48 h post-transfection, the cells were lysed with 200 µl lysis buffer containing 150 mM sodium chloride 1.0% Triton X-100 and 50 mM Tris, pH 8.0 supplemented with Mini, EDTA-free Protease Inhibitor Cocktail (Roche), rotated at 4°C until observation of DNA strings (around 30 min). The lysate was centrifuged at 12 000 rcf for 10 min and the supernatant was harvested. For RNase A treatment, lysate was incubated with RNase A (Invitrogen) at a final concentration of 50 µg/ml for 1 h at 4°C. 10 µl of the lysate was saved as input and the remaining lysate was added to 25 µl of Streptavidin Agarose (Pierce, Cat# 20347) respectively with rotation at 4°C for 2 h. The beads were subsequently harvested by centrifugation and 10 µl of supernatant was collected as post pulldown fraction. The beads were subsequently washed four times with the same lysis buffer without protease inhibitor. The input, pull-down and post pull-down fraction were boiled with 25 µl 2× loading buffer prior to SDS-PAGE. The ADAR2 protein was detected with mouse (ms) anti-FLAG antibody (Sigma-Aldrich, Cat# F1804) and the SRSF9 and relevant variants were detected with rabbit (rb) anti-HA antibody (Sigma-Aldrich, Cat# H6908).

Real-time quantitative PCR

The real-time qPCR reactions consisted of 2 µl of the pre-amplified cDNA, 10 µl of 2× Taqman Universal PCR Master Mix (Applied Biosystem, 4304437, USA), 1 µl of 20× Taqman gene expression assay (Applied Biosystem, USA) and made up to a final volume of 20 µl with sterile water. The real time PCR reactions were run on the Applied Biosystems 7500 Real-Time PCR System. Cycling conditions were as follow: 50°C for 2 min, 95°C for 10 min and 40 cycles of 95°C for 15 s followed by at 60°C for 1 min. All experiments were performed in triplicate. The Ct values were computed with the comparative quantitation method in Applied Biosystems 7500 Software v2.3. The Ct of two targets (ADAR2, Mm00504621_m1 and SRSF9, Mm00470546_m1, Applied Biosystem, USA) was normalized to the Ct of the reference genes (GAPDH, Mm99999915_g1, Applied Biosystem, USA). Delta Ct values are calculated with the formula Ctreference – Cttarget.

Enhanced CLIP experiments

HEK 293 cells cultured to 50% confluency in 10 cm plates were co-transfected with 0.4 µg of minigene gIQEQ, 1.0 µg of TAG construct and 4 µg of HA-tagged SRSF9 (HA-SRSF9). Approximately 48 h post-transfections, the cells were UV crosslinked (400 mJ/cm^2 constant energy) and immediately pelleted and frozen on dry ice. eCLIP procedure was performed as described (30). Briefly, the cell pellets were lysed in eCLIP lysis buffer and sonicated (BioRuptor).

Lysates were treated with RNase I (Ambion) to fragment the RNA. One-tenth of the lysate was saved as input sample. The remaining lysate was incubated with antibodies against HA (Sigma-Aldrich, H6908) to immunoprecipitate SFSF9-RNA complexes. Immunopreciptate (IP) samples were subjected to a series of stringent washes, followed by dephosphoralyation of RNA by FastAP (Fermentas) and T4 Kinase (NEB), and ligation of a 3' RNA adapter with T4 RNA Ligase (NEB). Immunoprecipitates and input samples were separated by SDS-PAGE, transferred to nitrocellulose membrane, and then the region of membrane corresponding to 25–100 kDa was excised for each immunoprecipitate and input sample. Input samples are referred to as size-matched input (SMInput) controls. RNA was isolated from the membrane, reverse transcribed with AffinityScript (Agilent), free primers were removed (ExoSap-IT, Affymetrix), and a DNA adaptor was ligated onto the cDNA product with T4 RNA ligase (NEB). Libraries were then amplified with Q5 PCR mix (NEB), size selected using AMPure XP beads (Beckman Coulter, Inc.) and on a 3% agarose gel, and then quantified by qPCR (NEBNext Library Quant Kit, NEB) and with a Bioanalyzer instrument (Agilent). eCLIP-seq for HA-SFSR9 was performed in biological duplicates including SMInput duplicates. Sequencing was performed on Illumina NextSeq 500 (1st base, Singapore) with 260 million paired-ends, 50 bp reads/sample.

Analysis of eCLIP data

The downstream analysis of eCLIP data follow two previous eCLIP studies (30,31). Briefly, eCLIP sequencing reads were processed in five major steps: Firstly, all the paired-end reads were adaptor trimmed with cutadapt (v1.9.1). Subsequently, reads were mapped against repetitive elements (RepBase18.05) using STAR (v2.4.0i) with mapped reads discarded. Thirdly, the remaining reads were mapped to the appropriate genome, namely human genome (hg19) or mouse genome (mm10) with STAR (v2.4.0i). Only uniquely mapped reads were retained for downstream analysis. Next, PCR duplicates were removed with the help of a random-mer sequence in the eCLIP-seq adapter. Lastly, peak calling was performed with the CLIPper algorithm (32) using the second read of each paired-end reads.

To measure the peak enrichment over paired SMInput, the number of reads mapped to each peak's genomic region were obtained for both eCLIP sample and its paired SMInput. Fold-enrichment of each peak was then calculated as the ratio between the number of reads in eCLIP versus SMInput, normalized by usable read (uniquely mapped and post-PCR duplicates removal) depth in both samples. *P* values were calculated by Yates' Chi-Square test or Fisher's Exact Test (if the number of reads is <5 in CLIP or SMInput). If two peaks overlapped, the peak with the most significant enrichment over SMInput was retained. For the region-based analysis, usable reads on each genomic region for all transcripts annotated in UCSC knownGene table were counted. Only regions with >10 reads in one of CLIP or SMInput samples were considered. Similarly, CLIPper-identified peaks are also assigned to different genomic regions of each gene. Fold-enrichment and corresponding

significance were determined with the methods described above.

Drug preparation

10 mg/ml stock solutions of cycloheximide (Sigma-Aldrich, C7698) were prepared in distilled water and subsequently diluted in culture medium to10 µg/ml.

Immunofluorescence and microscopy

The rat cortical neurons were fixed with 4% PFA for 15 min, permeabilized with PBS containing 0.2% Tween-20 for 15 min and blocked with 10% FBS/PBS for 20 min. The cells were treated with mouse anti-HA antibody (Sigma-Aldrich Cat# H3663) and rabbit anti-ADAR2 (Abcam, ab64830) at 1:1000 dilution in 5% FBS/PBS at 4°C overnight and subsequently stained with goat anti-rabbit Alexa Fluor 594-conjugated antibody (Thermofisher Scientific Cat# A-11011) and goat anti-mouse Alexa Fluor 488-conjugated antibody (Thermofisher Scientific Cat# A-11029) at 1:300 dilution in 5% FBS/PBS at room temperature for 60 min. Subsequently the cells were incubated with Hoechst 33258 (Thermofisher Scientific Cat# H1398) 1:300 dilution in PBS for 10 min, mounted, air dried and examined with Olympus confocal FV3000 microscope.

RESULTS

Exon-intron RNA duplex underlies A-to-I RNA editing of Ca$_V$1.3

A-to-I RNA editing occurs via direct interaction of ADAR2 with the double-stranded RNA that is formed between the edited site and a complementary ECS sequence usually located in flanking introns. Such RNA duplex structures have been consistently observed in all ADAR2 substrates identified so far (13,33–36). Identifying a similar structure would not only validate editing of Ca$_V$1.3 transcripts but also shed light on how its editing is specifically regulated.

To this end, mouse genomic DNA sequence of *Cacna1d* gene (Genbank access no. NT_039606.7) that codes for Ca$_V$1.3 transcripts was modeled by Mfold webserver (http://mfold.bioinfo.rpi.edu/cgi-bin/rna-form1.cgi). The program detected an imperfect RNA duplex formed between exon 41 and a complementary sequence located 3700 nt upstream in the preceding intron (Figure 1A). The 40 base pair (bp) secondary hair-pin structure was disrupted by four bulges. Whereas the editable adenosine residues for the codons AT*A* and C*A*G lie in the stem structure between the second and third bulges from the left, the adenosine of the T*A*C codon is located in the second bulge (Figure 1A). Subsequently, *in silico* analysis was also performed with RNA sequences of human (Genbank access no. NW_921651.1) and rat (Genbank access no. NW_001084711). Reassuringly, similar RNA duplexes were also detected and subsequently sequence alignment revealed almost identical sequences in the ECS and exon 41 across all three species (Supplementary Figure S1).

In order to experimentally validate the predicted ECS, a minigene named gIQECS was generated by sub-cloning a
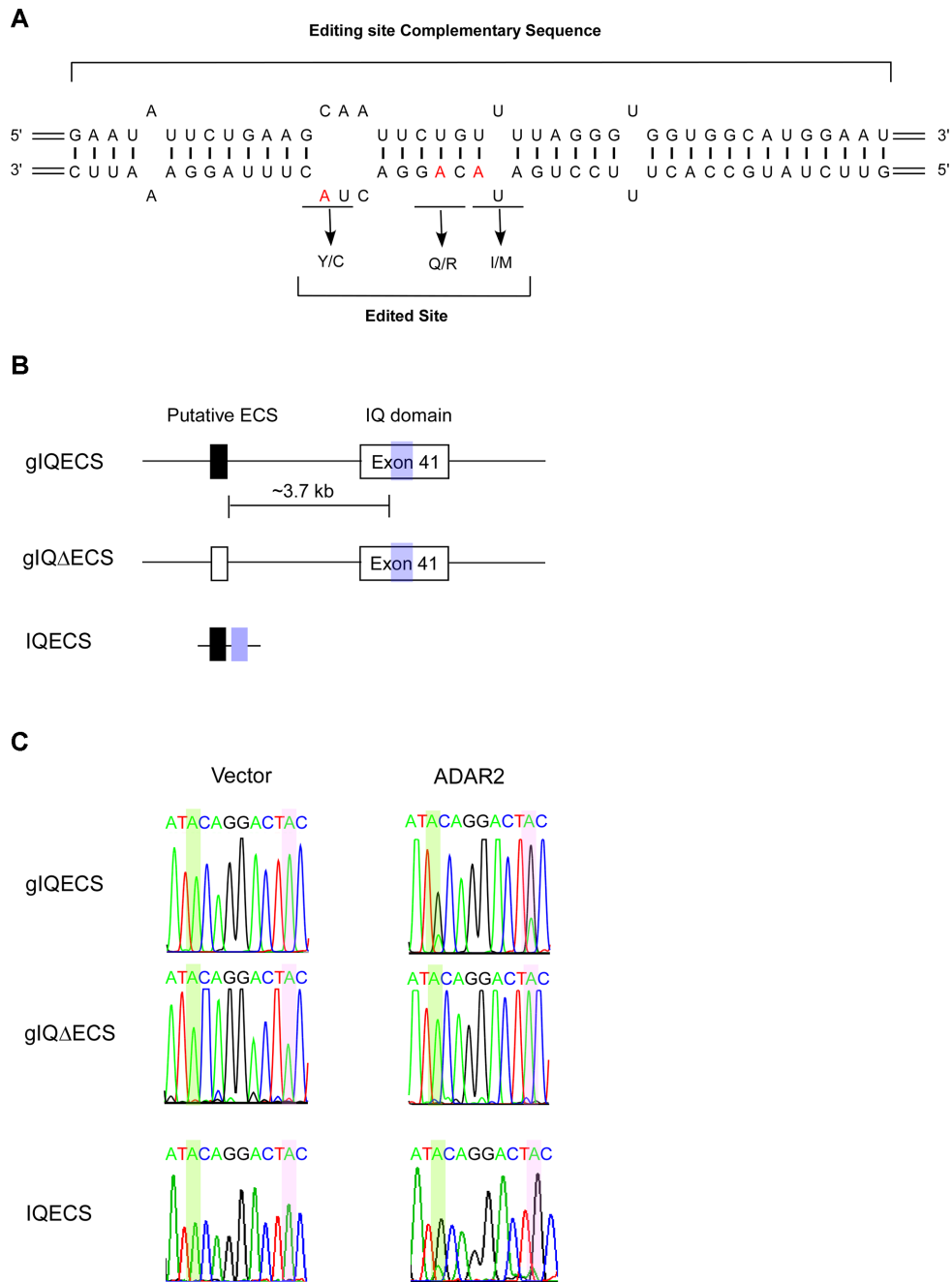
A

B

C

Figure 1. Identification of editing site complementary sequence (ECS) that facilitates the editing of Ca$_V$1.3. (**A**) RNA duplex structure formed between the edited site and an intronic complementary sequence as modeled by Mfold webserver (http://mfold.bioinfo.rpi.edu/cgi-bin/rna-form1.cgi). The edited adenosines were highlighted in red and arrows indicate respective amino acid changes. (**B**) Schematic diagram of the three minigenes of the mouse genomic fragment used for editing analysis. Top, gIQECS expressed a transcript that included the intact ECS, intermediate sequence and exon 41. The black and blue filled boxes indicate the position of putative ECS and its exonic complementary sequence respectively. Middle, the ECS sequence was deleted in the gIQΔECS minigene. Bottom, IQECS expressed a shorter transcript that retains only the ECS and its exonic complementary sequence separated by as short linker of 'CAGAG'. (**C**) Co-expression of respective minigenes with either empty pIRES2-EGFP vector control or ADAR2 in HEK293 cells. Top and bottom panels, chromatograms revealed robust editing in the ATA and TAC codon with gIQECS and IQECS minigenes. Middle, deletion of putative ECS in IQΔECS completely eliminated editing in both codons. The edited adenosine nucleotides of ATA and TAC codons were highlighted with translucent green and pink columns respectively.

4952 bp long mouse genomic sequence spanning the putative ECS, intermediate intronic sequence and exon 41 into the modified pRK5 expression vector (37). Subsequently, another minigene gIQΔECS was constructed by deleting the ECS in the gIQECS-containing plasmid (Figure 1B). Transient co-expression of full-length gIQECS with ADAR2 yielded robust editing in these codons within the IQ-domain: AT*A* to AT*G* and T*A*C to T*G*C; however, no significant editing was detected at the C*A*G codon (Figure 1C, top row). The results recapitulated the editing profile of native Ca$_V$1.3 transcripts in mouse neurons, whereby ATA and TAC codons were subjected to much higher level of editing as compared to the CAG codon (16). Furthermore, increased co-transfected levels of ADAR2 enhanced the level of editing in both codons (Supplementary Figure S2A). Gratifyingly, deletion of the predicted ECS sequence completely eliminated editing (Figure 1c, middle) which could not be compensated for by co-transfection with increased amounts of ADAR2 (Supplementary Figure S2B). Interestingly, editing of ATA and TAC codons remained unaffected with a much shorter transcript IQECS that contains only the ECS and edited sequence (Figure 1C, bottom), further validating the predicted ECS is correct and allowing the definition of a minimal structure required for ADAR2-mediated RNA editing of the IQ-domain of the Ca$_V$1.3 transcripts.

SRSF9 suppresses ADAR2 mediated A-to-I editing of Ca$_V$1.3

Equipped with the reporter assay for Ca$_V$1.3 editing, we then proceeded to screen for factors that could influence this molecular event. We first tested the effects of RPS14, SRSF9 and DHX15 (24) by co-transfecting them individually with ADAR2 and the gIQECS minigene. Strikingly, SRSF9 drastically attenuated the editing level of both ATA and TAC codons to only $12.91 \pm 1.47\%$ and $7.72 \pm 1.51\%$, respectively as normalized against control experiment in which a similar amount of ADAR2 was transfected alone (Figure 2A). Variation of the amount of co-transfected SRSF9 yielded a clear dose-response relationship of decreasing editing level that corresponded to an increasing level of exogenous SRSF9 (Figure 2B). Conversely, increasing ADAR2 expression significantly reversed the suppressive effect of SRSF9 (Figure 2C), suggesting that the two RNA-binding proteins may compete for binding to the same RNA substrate. Interestingly, the inhibitory effect of SRSF9 was lost on the short minigene IQECS (Supplementary Figure S3A and B), indicating that SRSF9 exerts its effect via interacting with sequences outside of the ECS and its complementary editable sequence on exon 41. Moreover, SRSF9 still robustly inhibits editing from another minegene gE40-E41 that spans exon 40 to exon 41 (Supplementary Figure S3C and D). Consistent with the editing assay that employed the mouse minigene, over-expression of SRSF9 in neuroblastoma SH-SY5Y cell line also robustly suppressed ADAR2-mediated editing of the endogenous human Ca$_V$1.3 transcripts (Figure 2D).

In comparison to SRSF9, DHX15 exerted a modest inhibitory effect as the normalized editing levels of ATA and TAC codons were only reduced to $81.45 \pm 1.57\%$ and 76.81

$\pm 3.23\%$ respectively, while RPS14 had no effect (Figure 2A) and transfection of increasing amounts of DHX15 and RPS14 did not further decrease the editing levels (Supplementary Figure S4A and B). Subcellular fractionation followed by western blot analysis revealed robust expression of hemagglutinin (HA) tagged DHX15 and RPS14 in both nuclear and cytoplasmic fractions of transfected the cells (Supplementary Figure S4C).

Suppressive effect of SRSF9 requires RNA binding

The SRSF9 protein possesses modular domains with two N-terminal RNA recognition motifs (RRM) including a canonical RRM1 and a pseudo-RRM2, followed by a C-terminal serine-arginine-rich (RS) domain. While RRM1 and RRM2 are each capable of RNA binding, the RS domain could be subjected to phosphorylation and has been shown to be involved in the regulation of alternative splicing via interaction with other SR protein factors in the spliceosome (38). To delineate these two functional roles, we assayed the contribution of the respective domains of SRSF9 in the suppression of Ca$_V$1.3 editing. Firstly, SRSF9_RRM12 mutant that was deleted of the RS domain retained its suppressive effect on Ca$_V$1.3 editing (Figure 3A and B) suggesting that recruitment of the SR protein is dispensable. Secondly, the motifs including FDVF in RRM1 and SWQDLKD in RRM2 have been reported to be critical for RNA binding by SRSF9. Specifically, substitutions of two phenylalanine residues in the *F*DV*F* motif of RRM1 to aspartate (FF-DD) have been reported to completely abolish RNA binding of RRM1 (39), while serine, tryptophan, glutamine, lysine and aspartate of the *SWQ*DL*KD* motif of RRM2 have also been shown to be important direct interaction with RNA (40). Here, FF-DD and/or *SWQ*DL*KD* to *AAA*DL*AA* (named '5A') substitutions were generated in the full length SRSF9 (Figure 3A). Notably, FF-DD substitutions attenuated the repressive function of SRSF9 drastically while the mutants harboring 5A or a combination of FF-DD and 5A mutations were completely unable to suppress editing. These results strongly suggest that for the repressive function of SRSF9 to be effective, it required synergy between both RRM domains (Figure 3B). Reassuringly, Western blot experiments detected robust expressions of WT SRSF9 and its deleted or point-mutants in both nuclear and cytoplasmic fractions (Figure 3C), substantiating the notion that nuclear SRSF9 or RRM domains repressed editing.

It has been reported that SRSF9 could interact with ADAR2 (24). However, it is not known if the domain of SRSF9 that interacts with ADAR2 is also important for its inhibitory effect on ADAR2 mediated RNA editing. In the current study, ADAR2 was tagged with streptavidin binding peptide (SBP) to generate ADAR2-SBP protein which could then be isolated through binding to streptavidin–agarose beads. Importantly, a very small amount of SRSF9 was pull-downed with transfection of SRSF9 alone as compared to both input and post pull-down fractions (Figure 3d). Upon co-transfection with ADAR2, SRSF9 could be pulled-down robustly. Interestingly, treatment with RNAase A to digest away a majority of RNA in the lysate appeared to further increase the amount of SRSF9 being
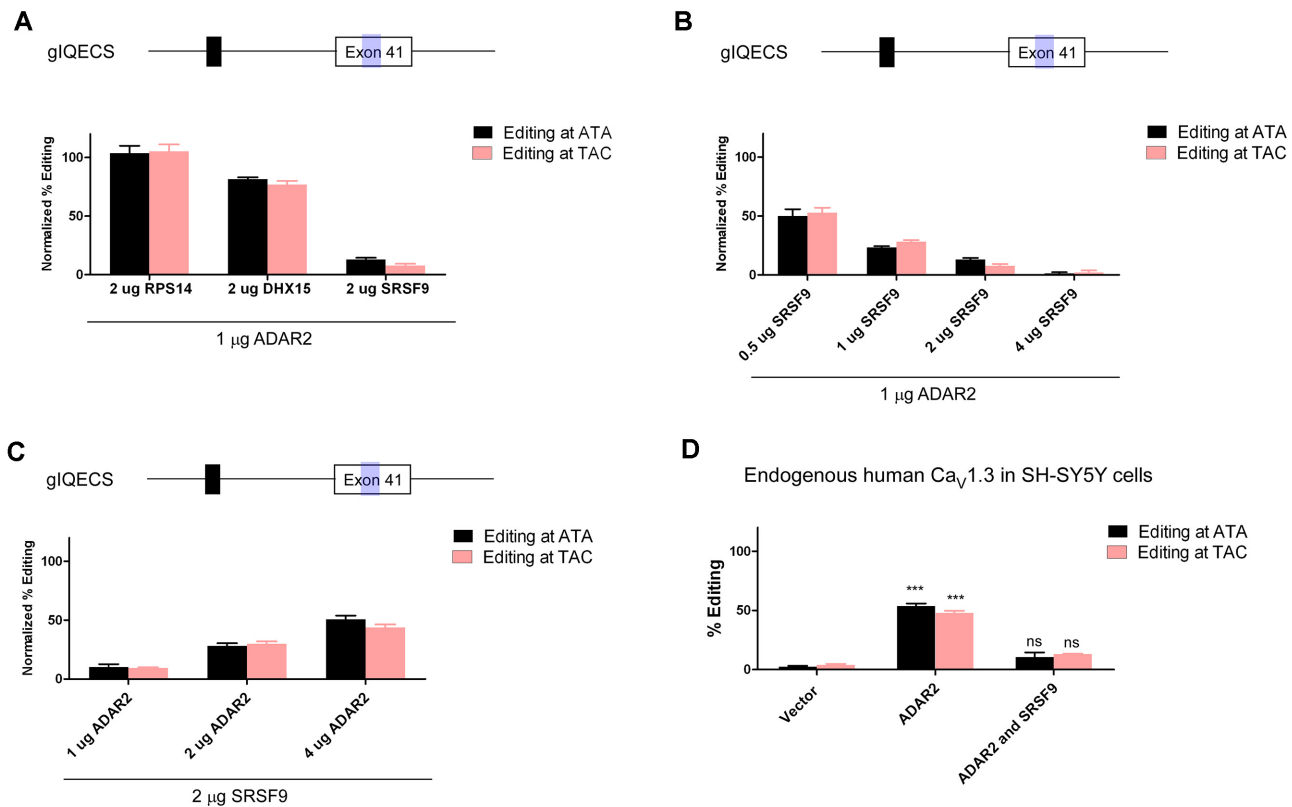
Figure 2. Suppression of ADAR2-mediated editing of Ca$_V$1.3 by SRSF9. (**A**) Top, schematic diagram of gIQECS minigene reproduced from Figure 1B. Bottom, bar chart reporting ADAR2-mediated editing of the transcripts expressed by full-length gIQECS minigene upon co-expression with RPS14, DHX15, and SRSF9 in heterologous HEK293 expression system. Editing of ATA and TAC codons were normalized against ADAR2 transfection alone, before averaging. Values shown are mean ± S.E. ($n = 3$). (**B**) Normalized editing level upon co-expression of increasing amount of SRSF9 with the same amount of ADAR2 as in (A). (**C**) Normalized editing level upon co-transfection of 1, 2 and 4 μg of ADAR2 in the presence of 2 μg of SRSF9, format as in (A). (**D**) Over-expression of ADAR2 in neuroblastoma SH-SY5Y cells significantly increased the editing level of endogenous human Ca$_V$1.3 IQ-domain which could be suppressed with co-expression of SRSF9. Bar chart reporting the percent editing at ATA and TAC codon of human Ca$_V$1.3 under respective conditions. ***$P < 0.001$ and ns, non-significant as compared to the vector control (Student's unpaired t-test) Values shown are mean ± S.E. ($n = 3$).

pulled-down, indicative of stronger ADAR2-SRSF9 interaction (Figure 3D and Supplementary Figure S5). Strikingly, deletion of the RS domain in SRSF9 abolished interaction between the two proteins while SRSF9 bearing mutations in either RRM1 (SRSF_FFDD) or RRM2 (SRSF9_5A) still binds to ADAR2. Lastly, mutation of both RRM domains in SRSF9 (SRSF9_FFDD-5A) significantly enhanced ADAR2–SRSF9 interaction, a trend similar to the RNase A treated samples. Taken together, while the RS domain is essential for the interaction between SRSF9 and ADAR2, it is not required for the inhibitory effect of SRSF9 on ADAR2-mediated editing. However, interaction between SRSF9 with ADAR2 does not affect the ADAR2-mediated Ca$_V$1.3 editing.

SRSF9 directly interacts with Ca$_V$1.3 minigene transcript

As a direct evidence to demonstrate that SRSF9 could bind to Ca$_V$1.3 transcript, we performed eCLIP followed by sequencing by co-transfecting HEK 293 cells with the gIQECS minigene and HA-tagged SRSF9. Reassuringly, mapping of the eCLIP-seq reads to the mouse genome (mm10) reports numerous interaction sites within the mini-

gene transcript (Figure 4). In particular, high significant peaks identified by CLIPper algorithm were found upstream of ECS and in the intronic regions between ECS and exon 41. Mapping of the reads to the human genome (hg19) on the other hand provided a more comprehensive view of the data. Notably, high reproducibility is found between the two biological replicates, with a high correlation ($R^2 \geq 0.55$) of their fold-enrichment of read counts in the CLIP sample in comparison to the paired SMInput within each region (Supplementary Figure S7A). We next identified 1,462 accurate SRSF9 binding sites on RNA targets shared with both replicates by discovering significantly enriched eCLIP peaks above SMInput ($P < 10^{-3}$, >8-fold) with the CLIPper algorithm (32) (Supplementary Figure S7B). SRSF9 binding sites are generally located in coding exons (CDS) and 5' UTR according to our eCLIP data (Supplementary Figure S7C) and they are significantly enriched in GA-rich motif (Supplementary Figure S6D), in agreement with a previous study (41).

Further analysis of the eCLIP-seq data revealed frequent binding of SRSF9 to the exon 4 of ADAR2 (Supplementary Figure S7A). Auto-editing of ADAR2 within the intron 3 particularly at -1 position creates novel 3' splice site and re-
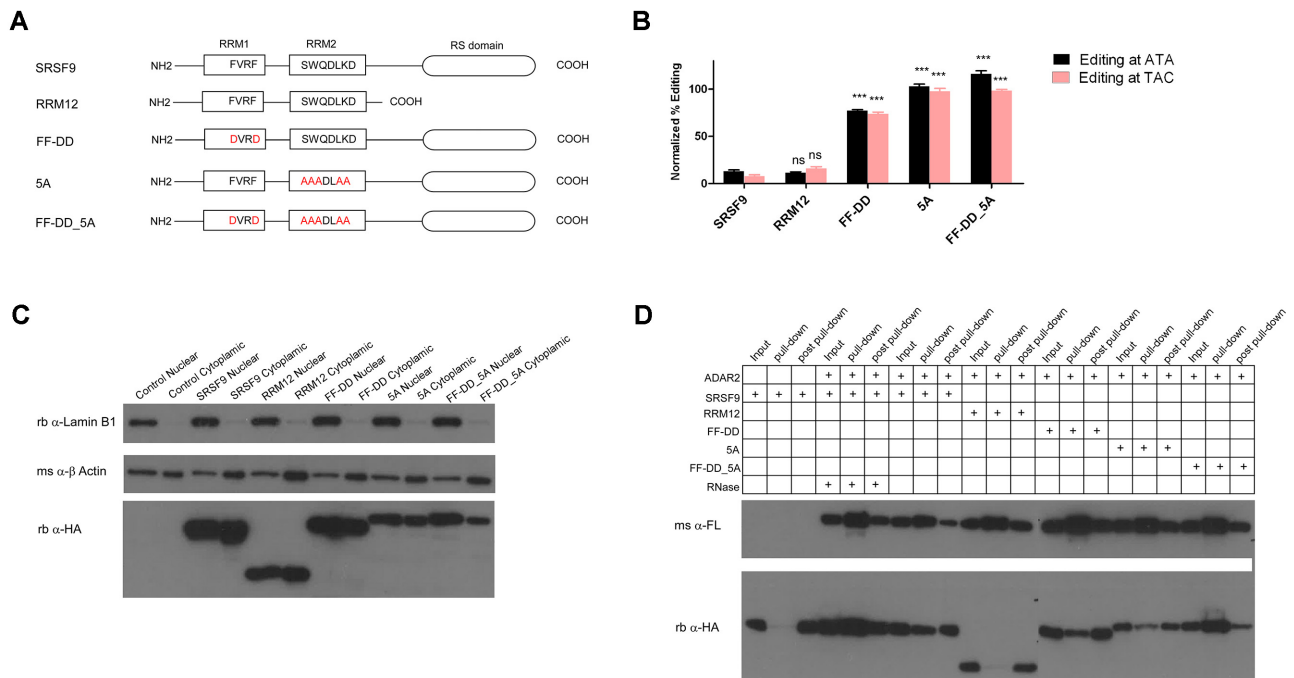
Figure 3. Suppressive effect of SRSF9 on Ca$_V$1.3 editing required intact RNA binding capability. (**A**) Schematic diagram depicting the deletions or point mutations of SRSF9. (**B**) Editing assay reporting the effect of deletion or point mutation of SRSF9 on ADAR2 mediated editing of the full-length gIQECS transcript. Editing of ATA and TAC codons were normalized against ADAR2 transfection alone before averaging. ***$P < 0.001$ and ns, non-significant as compared to the WT SRSF9 (Student's unpaired *t*-test) Values shown are mean ± S.E. ($n = 3$). The data for WT SRSF9 was reproduced from Figure 2A for comparison. (**C**) Western blot detect presence of HA-tagged SRSF9 and its different variants in both nuclear and cytoplasmic fraction. Nuclear envelop marker Lamin B1 and cytosolic protein β-Actin were used as nuclear and cytosolic marker respectively. The result is representative of three independent experiments. (**D**) Effect of RNase A treatment, deletion of RS domain and point mutation in either or both of RRM1 and 2 on the interaction between SRSF9 and ADAR2. Experiment was performed by pulling down ADAR2 tagged with both Flag (FL) and SBP tag with streptavidin-agarose beads. ADAR2 was detected with mouse (ms) anti-FL antibody and SRSF9 and its variants were detected with rabbit (rb) anti-HA antibody. Input, pull-down and post-pull down fractions were analysed for each condition. The result is representative of three independent experiments

sults in inclusion of additional 47 nucleotides (nt) upstream of exon 4, potentially leading to frameshifting and early truncation of ADAR2 (3,35). To test therefore if SRSF9 could modulate the auto-editing of ADAR2, HEK293 cells were transfected with either ADAR2 alone or ADAR2 together with SRSF9. Intriguingly, while RT-PCR from exon 3 to exon 4 detects robust inclusion of 47 nt upon transfection of ADAR2 in HEK293 cells, it was not observed in the cells transfected with vector alone and co-transfection of SRSF9 drastically diminished the inclusion of 47 nt (Supplementary Figure S7B and C). Further analysis by DNA sequencing of the RT-PCR products from intron 3 to exon 4 revealed robust editing at −28, −27, −1, 10, 23 and 24 positions upon expression of ADAR2, while editing was attenuated upon co-transfection of ADAR2 and SRSF9. No editing of ADAR2 transcript was observed in the cell transfected with vector alone, indicating low inherent expression of ADAR2 in HEK293 cells.

Downregulation of SRSF9 in neuronal tissues associated with lack of Ca$_V$1.3 editing

We have shown previously that Ca$_V$1.3 editing was restricted to neuronal tissues in brain and spinal cord. Consistently, in the current study, while editing was robustly detected in primary cortical neurons and various brain tissues such as brain cortex, hippocampus and cerebellum, Ca$_V$1.3

transcripts were largely unedited in several peripheral tissues such as heart, lung, adrenal gland, kidney and testis (Figure 5). Notably, editing of Ca$_V$1.3 mRNA was not observed in the cultured astrocytes (Figure 5), suggesting that RNA editing tailors unique Ca$_V$1.3 ion channel properties specifically to neuronal functions.

Given that editing of Ca$_V$1.3 could be robustly repressed by SRSF9, low expression of SRSF9 selectively in neurons would expectedly permit effective editing of Ca$_V$1.3 transcripts. To test this hypothesis, we performed real-time qPCR using RNA isolated from cultured mouse cortical neurons, astrocytes or from various tissues. Expectedly, *Adar2* mRNA was robustly detected in cultured cortical neurons and three different neuronal tissues including cortex, hippocampus and cerebellum. In comparison, its expression was significantly lower in astrocyte and peripheral tissues such as heart, adrenal gland and kidney while lung showed similar expression as cortical neurons and testis expressed high level of *Adar2* mRNA (Figure 6A). On the other hand, of *Srsf9* mRNA level are generally lower in neuronal tissues and heart as compared to astrocyte and other peripheral tissues.

At the protein level, expressions of ADAR2 and SRSF9 largely recapitulated the trend of their respective mRNA levels, as shown by Western blot analysis (Figure 6C). While strong signals were detected for ADAR2 in cortical neurons and three neuronal tissues, moderate levels were de-
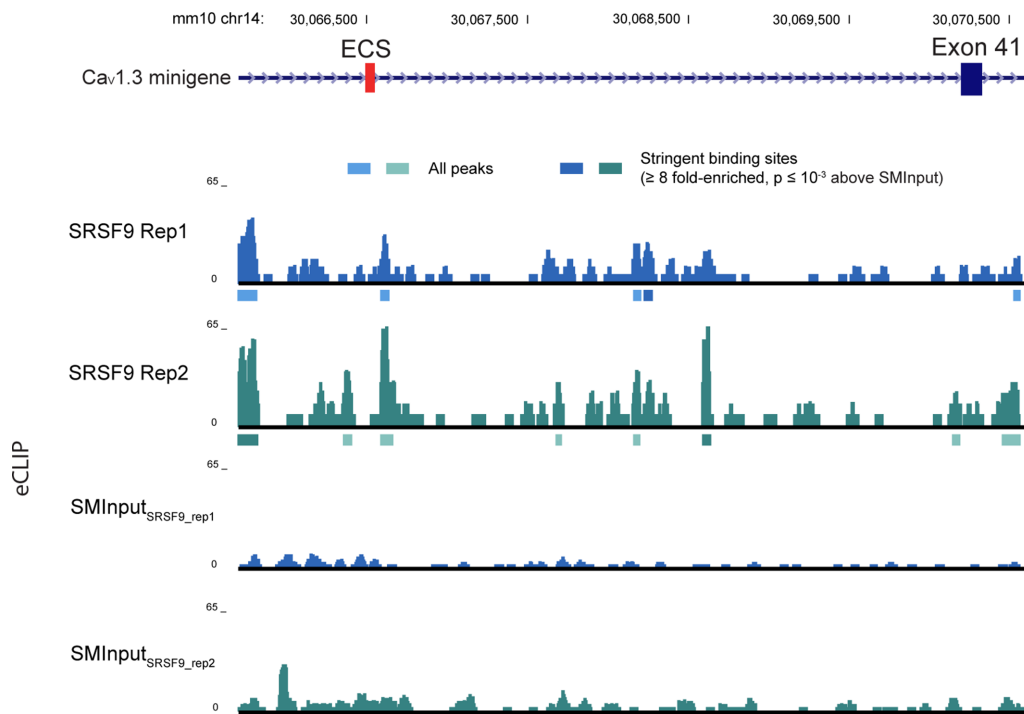
Figure 4. Detection of direct interaction between SRSF9 and Ca$_V$1.3 minigene transcript by eCLIP technique. SRSF9 eCLIP signals detected within the minigene. Reads density in reads per million usable (RPM) are shown for two replicates eCLIP and their coresponding size-matched input (SMInput) samples. All CLIPper-identified peaks are indicated as boxes below tracks, with dark colored boxes indicating significantly enriched binding sites above SMInput.

tected in astrocyte, lung and adrenal gland. Surprisingly, in testis only weak expression of ADAR2 was detected despite its high mRNA level. The level of ADAR2 protein was rather weak in heart and kidney tissue. In comparison, SRSF9 protein could barely be detected in neuronal tissues, heart and kidney. Strongest expression was found in testis and moderate expression was found in astrocyte, lung and adrenal gland (Figure 6C). Furthermore, RT-PCR analysis of *Srsf9* transcripts detected four distinct band sizes specifically in neuronal tissues, including the expected wild type (WT) *Srsf9* of 578 bp, indicative of the occurrence of alternative splicing of *Srsf9* transcripts specifically in neurons (Figure 6D). By contrast, only the *Srsf9* WT was dominantly expressed in cultured astrocytes and other peripheral tissues. Aberrant splicing could result in frame-shifting and yields transcripts with premature termination codons (PTC). Such mRNA can be detected by various nuclear surveillance mechanisms and subject to translational dependent degradation pathways such as non-sense mediated decay (NMD) (42). Mechanistically, aberrant splicing can therefore serve as a means to down-regulate transcript and protein expressions. To test if neuronal transcripts of *Srsf9* could be subjected to NMD, we treated the cortical neurons for 4 and 8 h with cycloheximide (CHX), a drug that blocked translation and therefore inhibited NMD. Intriguingly, as for *Srsf9*, intensity of the 668 bp band, as indicated by red arrow in Figure 6E, increased progressively with prolonged CHX incubation, while the intensity for the other bands did not change significantly, suggesting that some splice variants of *Srsf9* could indeed undergo NMD.

To account for the different variants of *Srsf9*, PCR products of *Srsf9* amplified from mRNA isolated from neurons after 8 h of CHX treatment were excised from agarose gel, purified, and cloned into plasmids for DNA sequencing. It turned out that alternate inclusion of exon 1a, exon 3 or both exons correlated with the higher PCR product sizes of 936, 668 and 1026 bp respectively (Figure 6F and Supplementary Figure S9). Importantly, *in silico* translation of cDNA sequences predicted premature termination codons (PTC) present in both exon 1a and exon 3 (Figure 6F and Supplementary Figure S8). Potentially, inclusion of exon 3 would therefore predispose the 668 bp transcript toward NMD as observed in Figure 6F, rather than supporting translation. Additionally, protein variants produced from alternative transcripts would be truncated due to PTCs, thereby drastically reducing the expression of functional *Srsf9* proteins.

Overexpression of SRSF9 in primary cortical neuronal culture supressed ADAR2 mediated editing of Ca$_V$1.3

Given the additional complexity of SRSF9 inhibiting ADAR2 mediated auto-editing, as an important experiment, we decided to overexpress SRSF9 in rat cortical neuronal culture that expressed endogenous ADAR2 and displayed robust editing of Ca$_V$1.3 and *Adar2*. The neurons were transduced with lentivirus that expressed either HA-tagged SRSF9$_{WT}$ or RNA binding mutant SRSF9$_{FF-DD\_5A}$ in addition to the control vector. Interestingly, significant reductions of editing in ATA and TAC codons were observed in neurons overexpressing SRSF9$_{WT}$, but not in the
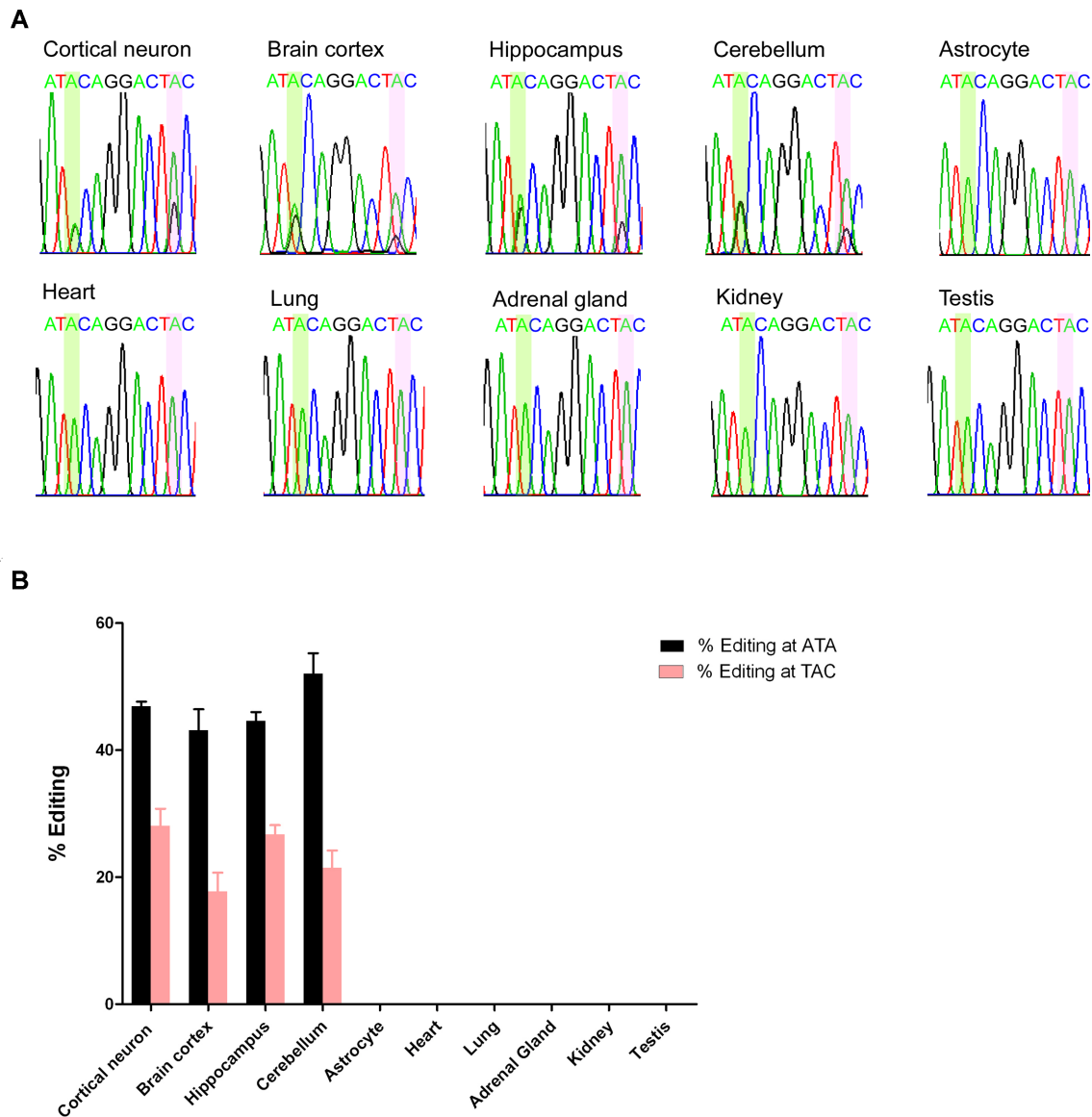
A

B

Figure 5. Tissue-selective editing of Ca$_V$1.3 transcripts. (**A**) Representative DNA sequencing chromatograms from direct analysis of RT-PCR products of primary culture of mouse cortical neurons, brain cortex, hippocampus, cerebellum, astrocytes and different peripheral tissues as indicated. The edited adenosine nucleotides of ATA and TAC codons were highlighted with translucent green and pink columns respectively. (**B**) Bar chart reporting the levels of editing of respective cultured cells and tissues. Percent editing at ATA and TAC codon, as calculated by dividing heights for adenosine peak over the total height of the overlapping adenosine and guanosine peaks. Values shown are mean ± S.E. ($n = 3$).

SRSF9$_{FF-DD\_5A}$ mutant, as compared to the control (Figure 7A). Reassuringly, Western blot detected robust expression of the HA-tagged proteins although the expression level for SRSF9$_{FF-DD\_5A}$ appeared to be lower as compared to SRSF9$_{WT}$ while the expression level of ADAR2 was not significantly affected (Figure 7B). Subsequent immunofluorescence staining reported nuclear localization of HA signals only in neurons transduced with HA-tagged SRSF9$_{WT}$ or SRSF9$_{FF-DD\_5A}$. Interestingly, punctate signals of ADAR2 in the nucleus suggests the localization of ADAR2 mostly in the nucleolus in neurons (Figure 7C). Moreover, analysis of RT-PCR product of *Adar2* also detected reduced editing at –1, 10 and 23 positions upon over-expression of SRSF9$_{WT}$,

correlating with a significantly reduced inclusion of 47-nt (Supplementary Figure S9)

DISCUSSION

A-to-I editing is highly enriched among neural tissues and mis-regulation of editing are associated with a wide range of neurological disorders including mood disorder, amyotrophic lateral sclerosis, glioma and Alzheimer's disease. Editing within exon 41 of Ca$_V$1.3 transcript exemplifies many features of ADAR2 mediated A-to-I RNA editing, being developmentally regulated and neuron-specific. Furthermore, similar to all other ADAR2 targets discovered so far, a predicted RNA duplex structure formed between exonic and the intronic complementary ECS sequence dictates
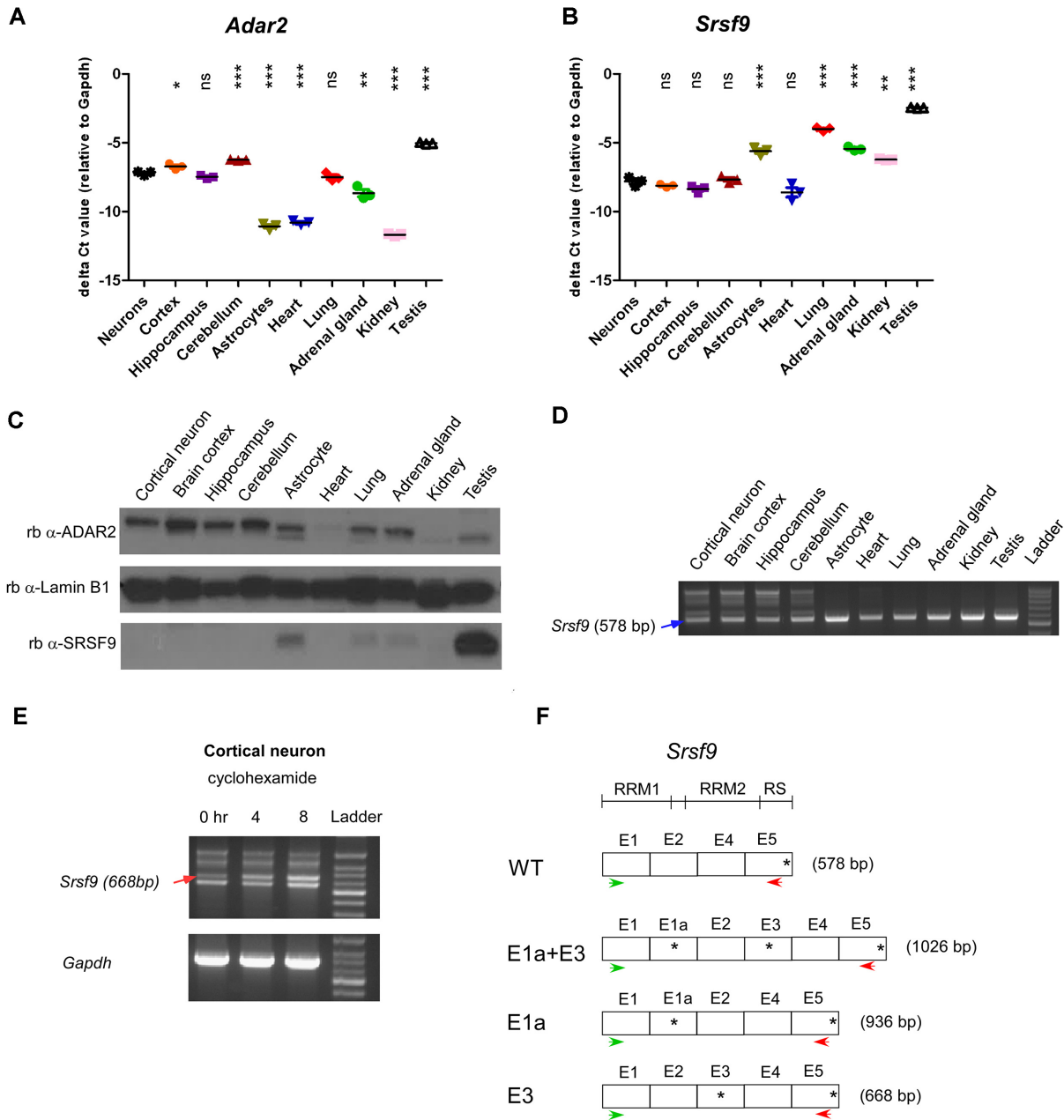
Figure 6. Tissue-selective expression pattern of *Adar2* and *Srsf9*. (**A**) Real-time qPCR reporting expression of mouse *Adar2* in cultured cortical neurons, brain cortex, hippocampus, cerebellum, astrocytes and other mouse tissues including heart, lung, adrenal gland, kidney and testis. The data was shown as delta Ct values are calculated with the formula Ct (*Adar2 – Gapdh*). ***$P < 0.001$ and ns, non-significant as compared to the cultured cortical neurons (Student's unpaired t-test) Values shown are mean $\pm$ S.E. ($n = 3$). (**B**) Real-time qPCR reporting expression of mouse *Srsf9*, format as in (A). (**C**) Western blot analyses of the expression ADAR2 and SRSF9. The nuclear envelop marker Lamin B1 was included as a loading control. The exemplary blots is representative of six independent experiments. (**D**) RT-PCR gel reporting the alternative splicing pattern of *Srsf9* exclusive in the cortical neurons and different neuronal tissues. (**E**) Treatment with 100 μg/ml cycloheximide detected translational depedent degradation of *Srsf9* mRNA as indicated by red arrow. The result is representative of three independent experiments. (**F**) Bacterial cloning and DNA sequencing identified four alternatively spliced variants of *Srsf9*. Top, mapping of different functional domains to respective exonic region in the WT *Srsf9* coding sequence. Alternative inclusion of either exon 1a (E1a) or exon 3 (E3) or both in *Srsf9* yielded three transcripts of 936, 668 and 1026 bp amplicon in addition to the 578 bp band as detected in (E) Asterixs denote the position of stop codons and the green and red arrows indicate the position of forward and reverse primers respectively used in (E).
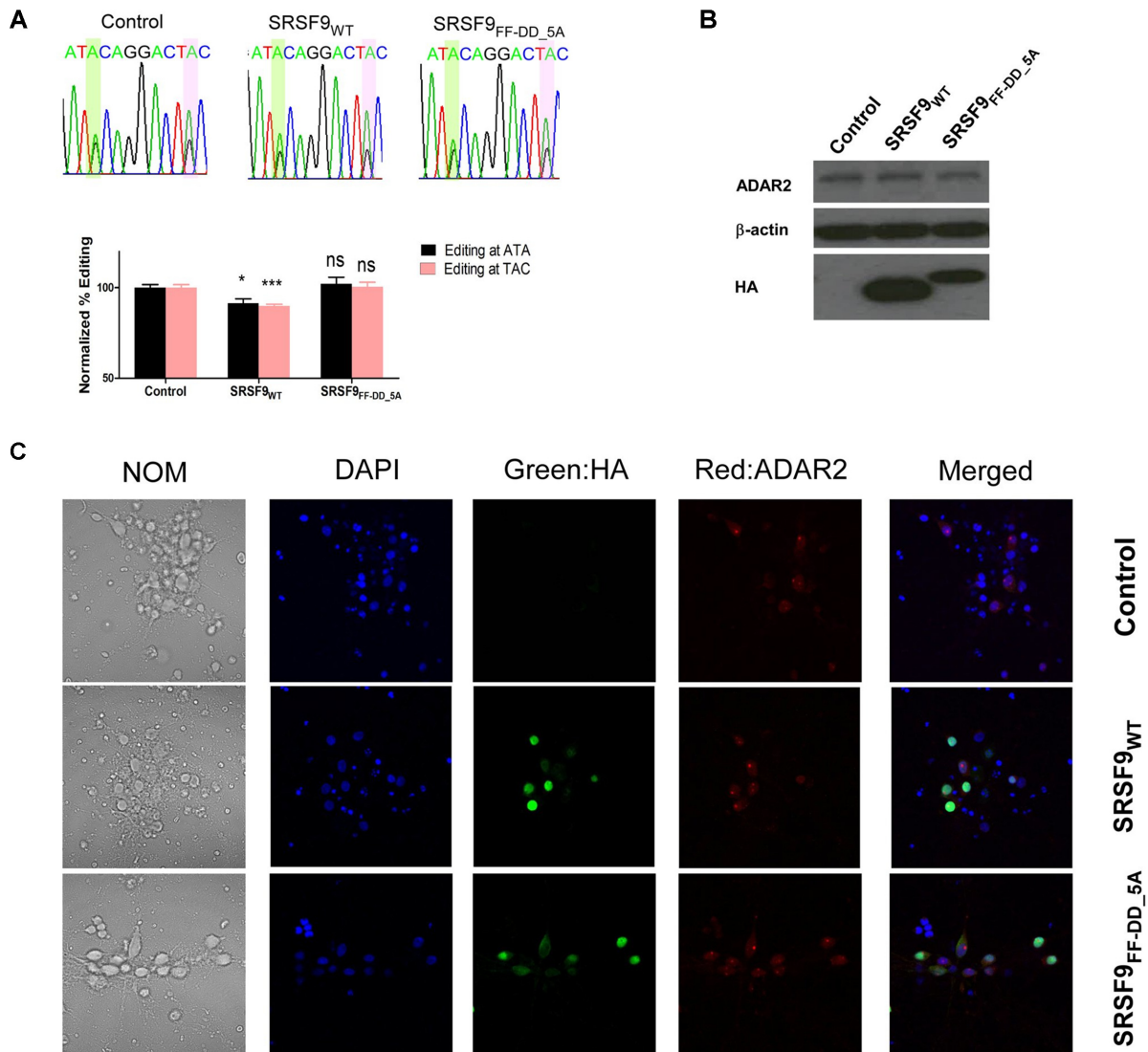
Figure 7. Overexpression of SRSF9 in primary cortical neurons reduced editing of *CaV1.3* RNA. (**A**) Top, representative DNA sequencing chromatograms from direct analysis of CaV1.3 RT-PCR products of primary culture of rat cortical neurons transduced with control or SRSF9WT or RNA binding mutant SRSF9FF-DD_5A. The edited adenosine nucleotides of were highlighted with translucent green and pink columns respectively. Bottom, bar chart reporting the levels of editing of respective types of cells. Editing of ATA and TAC codons were normalized against neurons transduced with control virus, before averaging. *$P < 0.05$, ***$P < 0.01$ and ns, nonsignificant as compared to control (Student's unpaired *t*-test) Values shown are mean $\pm$ S.E. ($n = 6$). (**B**) Western blot reporting the expression of ADAR2 and HA-tagged SRSF9WT or SRSF9FF-DD_5A. β-Actin was used as loading control. (**C**) Exemplar image of immunofluorescence staining detected the expression of endogenous ADAR2 and HA-tagged SRSF9WT or SRSF9FF-DD_5A.

editing within exon 41. Remarkably, sequences of both exon 41 and ESC are highly evolutionarily conserved, correlating with observed CaV1.3 editing in species such as human, mouse and rat. Experimentally, deletion of the ECS within the gIQECS minigene completely blocked editing of exon 41 while connecting the ECS directly to its complementary exonic sequence with minimal intermediate sequence was sufficient to support editing. Mice genetically targeted to remove the m*Cacna1d* ECS sequence showed complete abolishment of editing of exon 41 of the CaV1.3 channel (unpublished data), further supporting the role of the identified ECS as a cis-element fundamental to the editing of CaV1.3.

Given the ubiquitous expression of ADAR2 as detected by both RT-PCR and western blot in both neuronal tissues

and most of the peripheral tissues, it is therefore puzzling that a strict tissue-specific regulation exists to restrict editing of CaV1.3 transcripts to only neurons in the central nervous system. In contrast, ADAR2 has been shown to edit filamin A transcripts in many non-neuronal tissues as revealed by comparison between the WT and ADAR2 knockout mice, suggesting that editing of different ADAR substrates is regulated differently (43). Utilizing the minigene assay, we screened for regulatory factors, focusing on several RNA binding proteins including RPS14, DHX15 and SRSF9 that have been shown to inhibit ADAR2 activity. Significantly, SRSF9 was found to strongly suppress editing of both the CaV1.3 transcript encoded by the minigene

and the native human $Ca_V1.3$ transcript expressed in human neuroblastoma cell line SH-SY5Y.

SRSF9 belongs to a family of RNA binding serine/arginine (SR)-rich proteins that are involved in many different aspects of pre-mRNA processing including alternative splicing, nuclear export and translation. All SR proteins display modular structures with either one or two N-terminal RNA recognition motifs (RRM) followed by an arginine/serine rich RS domain. Although the RS domain engages in versatile protein-protein interactions that mediates spliceosomal assembly prior to splicing event, its requirement in splicing regulation seems to be RNA substrate dependent (44). This notion is supported by published data that indicated RRM2 alone was sufficient to mediate normal splicing for some of its targets (40). Therefore, in a competition model, it was proposed that SRSF9 could regulate exon inclusion/exclusion by displacing other splicing factors from binding to the same regulated splice site (40). Interestingly, while the RS domain also appears to be dispensable for SRSF9 to regulate ADAR2-mediated $Ca_V1.3$ editing, deletion of RS domain abolished interaction between SRSF9 and ADAR2. Rather, intact function of RNA binding domains inclusive of both the RRM1 and RRM2 is sufficient for their inhibitory effects as revealed by extensive deletions and point mutations within SRSF9. On the other hand, RS was found to be important for interaction between SRSF9 and ADAR2. Despite the previous suggestion that SRSF9 interaction with ADAR2 as a possible hypothesis to explain its suppression of ADAR2 activity, this may not be the case as SRSF9 FF-DD_5A mutant binds strongly to ADAR2 and yet fails to suppress ADAR2-mediated $Ca_V1.3$ editing. Remarkably, the ratio of ADAR2 to SRSF9 co-transfected determined the editing level of $Ca_V1.3$ editing; while increasing amount of SRSF9 suppressed $Ca_V1.3$ editing in a dose dependent manner, co-expression of increasing amount of ADAR2 in the presence of SRSF9 could reverse such inhibition. Hence, it is highly possible that SRSF9 regulates ADAR2-mediated $Ca_V1.3$ editing via competing with ADAR2 for the binding to the same RNA substrate or SRSF9 binding might interfere with the formation of the critical stem-loop structure formed by ECS-exon 41 sequences to allow ADAR2-mediated editing to occur. However, knockdown of endogenous SRSF9 or SRSF1, which is known to share a similar motif as SRSF9, or both could not further increase the editing of $Ca_V1.3$ minigene or the endogenous ADAR2 transcript in HEK 293 cells. More striking, knockdown of SRSF9, 1 or both led to a small decrease of editing as compared to the non-targeting siRNA transfected cells, suggesting a U-shape response. As SRSF9 interacts directly with ADAR2 and $Ca_V1.3$ RNA as revealed by the data in our current work, at the basal level, SRSF9 or SRSF1 could possibly recruit and facilitate RNA editing mediated by ADAR2. On the other hand, when SRSF9 is in abundance, they bind to multiple sites of the RNA resulting in disruption of the stem-loop structure, ADAR2 binding, and therefore reduced RNA editing of the CaV1.3 IQ-domain. The fine balance between recruitment of ADAR2 and disruption of stem-loop structure and ADAR2 binding will at some point result in maximal editing. Consistently, over-expression of mouse SRSF9 in

the presence of siRNA targeting endogenous SRSF9 almost completely abolished editing (Supplementary Figure S10).

SRSF9 was shown to display promiscuous binding patterns in both intronic and exonic sequence (38). Employing a comprehensive RNA competition assay, Ray *et al.*, 2013 reported that SRSF9 interacted favourably with purine rich heptamers (41). Remarkably, eCLIP-seq data revealed strong binding of SRSF9 particularly upstream of the ECS and in the intermediate sequence between ECS and exon 41. Importantly, further in silico analysis and molecular data in this current work suggests that SRSF9 could also affect auto-editing of ADAR2 in intron 3 by direct binding to exon 4 of ADAR2. Editing of ADAR2 at -1 position in intron 3 was known to create an addition splice site that introduced 47 nucleotides intronic sequence to the reading frame, potentially leading to frameshifting. While inefficient usage of alternate start codon could still produce functional ADAR2, abolishment of ADAR2 auto-editing in mice resulted in upregulation of ADAR2 expression (20), suggesting editing of ADAR2 is a negative feedback mechanism serving to regulate its own expression. In the more native context such as neurons, suppression of auto-regulatory editing of ADAR2 by SRSF9 could transiently yield more efficient wildtype ADAR2 mRNA allowing for more ADAR2 to be expressed. However, given the existence of such a negative feedback mechanism, ADAR2 would eventually buffer its own upregulation by editing its own transcript in the long run. Such temporal regulation may require more detailed analyses in the future. Interestingly, lower editing levels in *Adar2* and $Ca_V1.3$ were consistently observed upon over expression of wildtype SRSF9 in rat cortical neurons while expression of RNA binding mutant $SRSF9_{FF-DD\_5A}$ failed to suppress editing, suggesting again that SRSF9 suppresses ADAR2 mediated editing via direct interaction with the RNA targets. Despite the use of concentrated lentivirus, the transduction efficiency was ~40–50%, as estimated by comparing the green HA signal versus and the DAPI signal, and the intensity of the green signal varies from cell to cell. This is a limitation associated with the use of lentivirus for transfection of a heterogenous population of cortical neurons, and it has been shown that the efficiency of transfection is less than 10% for inhibitory neurons (45).

Strikingly, we observed that the neuronal transcripts of *Srsf9* were subjected to alternative splicing. Specifically, alternative inclusion of exon 1a and exon 3 in *Srsf9* introduced premature stop codons and could predispose such transcripts toward NMD or transcripts that produce non-functional truncated proteins. Neuron-specific alternative splicing could therefore lead to down-regulation of the protein-coding *Srsf9* WT mRNA level, as supported by the quantitative real-time PCR data. Consistently, the expression of SRSF9 protein in cultured cortical neurons and different brain tissues such as cortex, hippocampus and cerebellum could hardly be detected by western blot analyses as compared to peripheral tissues such as lung, adrenal gland and testis. Currently, neuron-specific mechanism that regulates the alternative splicing of *Srsf9* mRNA remains unknown. As alternative splicing itself is also dynamically regulated, it would be interesting to test in future if revers-

ing the alternative splicing of neuronal *Srsf9* mRNA under certain patho-physiological conditions could enhance SRSF9 protein level which will then lead to repression of ADAR2 mediated Ca$_V$1.3 editing. Of note, in astrocyte and other peripheral tissues including lung, adrenal gland and testis, both ADAR2 and SRSF9 protein could be readily detected. The presence of SRSF9 could therefore serve to regulate ADAR2-mediated Ca$_V$1.3 editing in such tissues. However, the lack of editing in heart and kidney could largely be attributed to very low expression of ADAR2. In summary, this study thus identified a novel mechanism whereby RNA binding splicing factor SRSF9 specifically restricted ADAR2 mediated A-to-I editing of Ca$_V$1.3 transcripts and potentially ADAR2 itself via direct interaction with its RNA substrate. Variation in the expression of SRSF9 could therefore contribute toward global change in A-to-I RNA editing profile under different physiological and clinical conditions.

DATA AVAILABILITY

The accession number for the eCLIP sequencing data deposited in GEO for this paper is GSE113193.

SUPPLEMENTARY DATA

Supplementary Data are available at NAR Online.

ACKNOWLEDGEMENTS

FUNDING

REFERENCES

1. Rebagliati,M.R. and Melton,D.A. (1987) Antisense RNA injections in fertilized frog eggs reveal an RNA duplex unwinding activity. *Cell*, **48**, 599–605.
2. Bass,B.L. and Weintraub,H. (1987) A developmentally regulated activity that unwinds RNA duplexes. *Cell*, **48**, 607–613.
3. Rueter,S.M., Dawson,T.R. and Emeson,R.B. (1999) Regulation of alternative splicing by RNA editing. *Nature*, **399**, 75–80.
4. Flomen,R., Knight,J., Sham,P., Kerwin,R. and Makoff,A. (2004) Evidence that RNA editing modulates splice site selection in the 5-HT2C receptor gene. *Nucleic Acids Res.*, **32**, 2113–2122.
5. Vesely,C., Tauber,S., Sedlazeck,F.J., Tajaddod,M., von Haeseler,A. and Jantsch,M.F. (2014) ADAR2 induces reproducible changes in sequence and abundance of mature microRNAs in the mouse brain. *Nucleic Acids Res.*, **42**, 12155–12168.
6. Kume,H., Hino,K., Galipon,J. and Ui-Tei,K. (2014) A-to-I editing in the miRNA seed region regulates target mRNA selection and silencing efficiency. *Nucleic Acids Res.*, **42**, 10050–10060.
7. Kawahara,Y., Zinshteyn,B., Sethupathy,P., Iizasa,H., Hatzigeorgiou,A.G. and Nishikura,K. (2007) Redirection of silencing targets by adenosine-to-inosine editing of miRNAs. *Science*, **315**, 1137–1140.
8. Nishikura,K. (2006) Editor meets silencer: crosstalk between RNA editing and RNA interference. *Nat. Rev. Mol. Cell Biol.*, **7**, 919–931.
9. Yang,W., Chendrimada,T.P., Wang,Q., Higuchi,M., Seeburg,P.H., Shiekhattar,R. and Nishikura,K. (2006) Modulation of microRNA processing and expression through RNA editing by ADAR deaminases. *Nat. Struct. Mol. Biol.*, **13**, 13–21.
10. Daniel,C., Lagergren,J. and Ohman,M. (2015) RNA editing of non-coding RNA and its role in gene regulation. *Biochimie*, **117**, 22–27.
11. Picardi,E., D'Erchia,A.M., Gallo,A., Montalvo,A. and Pesole,G. (2014) Uncovering RNA editing sites in long Non-Coding RNAs. *Front. Bioeng. Biotechnol.*, **2**, 64.
12. Wang,Q., Miyakoda,M., Yang,W., Khillan,J., Stachura,D.L., Weiss,M.J. and Nishikura,K. (2004) Stress-induced apoptosis associated with null mutation of ADAR1 RNA editing deaminase gene. *J. Biol. Chem.*, **279**, 4952–4961.
13. Higuchi,M., Maas,S., Single,F.N., Hartner,J., Rozov,A., Burnashev,N., Feldmeyer,D., Sprengel,R. and Seeburg,P.H. (2000) Point mutation in an AMPA receptor gene rescues lethality in mice deficient in the RNA-editing enzyme ADAR2. *Nature*, **406**, 78–81.
14. Horsch,M., Seeburg,P.H., Adler,T., Aguilar-Pimentel,J.A., Becker,L., Calzada-Wack,J., Garrett,L., Gotz,A., Hans,W., Higuchi,M. *et al.* (2011) Requirement of the RNA-editing Enzyme ADAR2 for Normal Physiology in Mice. *J. Biol. Chem.*, **286**, 18614–18622.
15. Slotkin,W. and Nishikura,K. (2013) Adenosine-to-inosine RNA editing and human disease. *Genome Med.*, **5**, 105.
16. Huang,H., Tan,B.Z., Shen,Y., Tao,J., Jiang,F., Sung,Y.Y., Ng,C.K., Raida,M., Kohr,G., Higuchi,M. *et al.* (2012) RNA editing of the IQ domain in Ca(v)1.3 channels modulates their Ca(2)(+)-dependent inactivation. *Neuron*, **73**, 304–316.
17. Khermesh,K., D'Erchia,A.M., Barak,M., Annese,A., Wachtel,C., Levanon,E.Y., Picardi,E. and Eisenberg,E. (2016) Reduced levels of protein recoding by A-to-I RNA editing in Alzheimer's disease. *RNA*, **22**, 290–302.
18. Peng,P.L., Zhong,X., Tu,W., Soundarapandian,M.M., Molner,P., Zhu,D., Lau,L., Liu,S., Liu,F. and Lu,Y. (2006) ADAR2-dependent RNA editing of AMPA receptor subunit GluR2 determines vulnerability of neurons in forebrain ischemia. *Neuron*, **49**, 719–733.
19. Agranat,L., Sperling,J. and Sperling,R. (2010) A novel tissue-specific alternatively spliced form of the A-to-I RNA editing enzyme ADAR2. *RNA Biol.*, **7**, 253–262.
20. Feng,Y., Sansam,C.L., Singh,M. and Emeson,R.B. (2006) Altered RNA editing in mice lacking ADAR2 autoregulation. *Mol. Cell. Biol.*, **26**, 480–488.
21. Gerber,A., O'Connell,M.A. and Keller,W. (1997) Two forms of human double-stranded RNA-specific editase 1 (hRED1) generated by the insertion of an Alu cassette. *RNA*, **3**, 453–463.
22. Marcucci,R., Brindle,J., Paro,S., Casadio,A., Hempel,S., Morrice,N., Bisso,A., Keegan,L.P., Del Sal,G. and O'Connell,M.A. (2011) Pin1 and WWP2 regulate GluR2 Q/R site RNA editing by ADAR2 with opposing effects. *EMBO J.*, **30**, 4211–4222.
23. Jacobs,M.M., Fogg,R.L., Emeson,R.B. and Stanwood,G.D. (2009) ADAR1 and ADAR2 expression and editing activity during forebrain development. *Dev. Neurosci.*, **31**, 223–237.
24. Tariq,A., Garncarz,W., Handl,C., Balik,A., Pusch,O. and Jantsch,M.F. (2013) RNA-interacting proteins act as site-specific repressors of ADAR2-mediated RNA editing and fluctuate upon neuronal stimulation. *Nucleic Acids Res.*, **41**, 2581–2593.
25. Huang,H., Yu,D. and Soong,T.W. (2013) C-terminal alternative splicing of CaV1.3 channels distinctively modulates their dihydropyridine sensitivity. *Mol. Pharmacol.*, **84**, 643–653.
26. Okun,E., Arumugam,T.V., Tang,S.C., Gleichmann,M., Albeck,M., Sredni,B. and Mattson,M.P. (2007) The organotellurium compound ammonium trichloro(dioxoethylene-0,0') tellurate enhances neuronal survival and improves functional outcome in an ischemic stroke model in mice. *J. Neurochem.*, **102**, 1232–1241.
27. Chan,E.S., Shetty,M.S., Sajikumar,S., Chen,C., Soong,T.W. and Wong,B.S. (2016) ApoE4 expression accelerates hippocampus-dependent cognitive deficits by enhancing Abeta

impairment of insulin signaling in an Alzheimer's disease mouse model. *Sci. Rep.*, **6**, 26119.

28. Walter,D.M., Venancio,O.S., Buza,E.L., Tobias,J.W., Deshpande,C., Gudiel,A.A., Kim-Kiselak,C., Cicchini,M., Yates,T.J. and Feldser,D.M. (2017) Systematic in vivo inactivation of Chromatin-Regulating enzymes identifies Setd2 as a potent tumor suppressor in lung adenocarcinoma. *Cancer Res.*, **77**, 1719–1729.

29. Kim,J.H., Chang,T.M., Graham,A.N., Choo,K.H., Kalitsis,P. and Hudson,D.F. (2010) Streptavidin-Binding peptide (SBP)-tagged SMC2 allows single-step affinity fluorescence, blotting or purification of the condensin complex. *BMC Biochem.*, **11**, 50.

30. Van Nostrand,E.L., Pratt,G.A., Shishkin,A.A., Gelboin-Burkhart,C., Fang,M.Y., Sundararaman,B., Blue,S.M., Nguyen,T.B., Surka,C., Elkins,K. *et al.* (2016) Robust transcriptome-wide discovery of RNA-binding protein binding sites with enhanced CLIP (eCLIP). *Nat. Methods*, **13**, 508–514.

31. Conway,A.E., Van Nostrand,E.L., Pratt,G.A., Aigner,S., Wilbert,M.L., Sundararaman,B., Freese,P., Lambert,N.J., Sathe,S., Liang,T.Y. *et al.* (2016) Enhanced CLIP uncovers IMP Protein-RNA targets in human pluripotent stem cells important for cell adhesion and survival. *Cell Rep.*, **15**, 666–679.

32. Lovci,M.T., Ghanem,D., Marr,H., Arnold,J., Gee,S., Parra,M., Liang,T.Y., Stark,T.J., Gehman,L.T., Hoon,S. *et al.* (2013) Rbfox proteins regulate alternative mRNA splicing through evolutionarily conserved RNA bridges. *Nat. Struct. Mol. Biol.*, **20**, 1434–1442.

33. Bhalla,T., Rosenthal,J.J., Holmgren,M. and Reenan,R. (2004) Control of human potassium channel inactivation by editing of a small mRNA hairpin. *Nat. Struct. Mol. Biol.*, **11**, 950–956.

34. Burns,C.M., Chu,H., Rueter,S.M., Hutchinson,L.K., Canton,H., Sanders-Bush,E. and Emeson,R.B. (1997) Regulation of serotonin-2C receptor G-protein coupling by RNA editing. *Nature*, **387**, 303–308.

35. Dawson,T.R., Sansam,C.L. and Emeson,R.B. (2004) Structure and sequence determinants required for the RNA editing of ADAR2 substrates. *J. Biol. Chem.*, **279**, 4941–4951.

36. Olson,P.A., Tkatch,T., Hernandez-Lopez,S., Ulrich,S., Ilijic,E., Mugnaini,E., Zhang,H., Bezprozvanny,I. and Surmeier,D.J. (2005) G-protein-coupled receptor modulation of striatal CaV1.3 L-type Ca2+ channels is dependent on a Shank-binding domain. *J. Neurosci.*, **25**, 1050–1062.

37. Higuchi,M., Single,F.N., Kohler,M., Sommer,B., Sprengel,R. and Seeburg,P.H. (1993) RNA editing of AMPA receptor subunit GluR-B: a base-paired intron-exon structure determines position and efficiency. *Cell*, **75**, 1361–1370.

38. Shepard,P.J. and Hertel,K.J. (2009) The SR protein family. *Genome Biol.*, **10**, 242.

39. Fu,Y., Huang,B., Shi,Z., Han,J., Wang,Y., Huangfu,J. and Wu,W. (2013) SRSF1 and SRSF9 RNA binding proteins promote Wnt signalling-mediated tumorigenesis by enhancing beta-catenin biosynthesis. *EMBO Mol. Med.*, **5**, 737–750.

40. Clery,A., Sinha,R., Anczukow,O., Corrionero,A., Moursy,A., Daubner,G.M., Valcarcel,J., Krainer,A.R. and Allain,F.H. (2013) Isolated pseudo-RNA-recognition motifs of SR proteins can regulate splicing using a noncanonical mode of RNA recognition. *Proc. Natl. Acad. Sci. U.S.A.*, **110**, E2802–E2811.

41. Ray,D., Kazan,H., Cook,K.B., Weirauch,M.T., Najafabadi,H.S., Li,X., Gueroussov,S., Albu,M., Zheng,H., Yang,A. *et al.* (2013) A compendium of RNA-binding motifs for decoding gene regulation. *Nature*, **499**, 172–177.

42. Garneau,N.L., Wilusz,J. and Wilusz,C.J. (2007) The highways and byways of mRNA decay. *Nat. Rev. Mol. Cell Biol.*, **8**, 113–126.

43. Stulic,M. and Jantsch,M.F. (2013) Spatio-temporal profiling of Filamin A RNA-editing reveals ADAR preferences and high editing levels outside neuronal tissues. *RNA Biol.*, **10**, 1611–1617.

44. Zhu,J. and Krainer,A.R. (2000) Pre-mRNA splicing in the absence of an SR protein RS domain. *Genes Dev.*, **14**, 3166–3178.

45. Nathanson,J.L., Yanagawa,Y., Obata,K. and Callaway,E.M. (2009) Preferential labeling of inhibitory and excitatory cortical neurons by endogenous tropism of adeno-associated virus and lentivirus vectors. *Neuroscience*, **161**, 441–450.